ACS Sustainable Chemistry & Engineering

pubs.acs.org/journal/ascecg

Research Article

Comparative Study on Electrochemical and Thermochemical Pathways for Carbonaceous Fuel Generation Using Sunlight and Air

Da Xu, Ian Sullivan, Chengxiang Xiang,* and Meng Lin*

Cite This: *ACS Sustainable Chem. Eng.* 2022, 10, 13945−13954

Read Online

ACCESS | Metrics & More | Article Recommendations | Supporting Information

ABSTRACT: A comparative study on the solar-to-fuel (STF) conversion efficiency of electrochemical and thermochemical approaches for methane (CH_4), methanol (MeOH), and ethanol (EtOH) generation using sunlight and air was performed. The system level STF conversion efficiency studied herein took into account of both the conversion processes and feedstock capture processes. In particular, the feedstock, CO_2 and H_2O, in this analysis were assumed to be captured from air. For thermochemical conversion, one and two-step approaches were considered including CH_4 generation from the Sabatier reaction, and two-step processes for methanol (MeOH) and ethanol (EtOH) generation from CO and H_2 coupled with the reverse water gas shift reaction (rWGS). State-of-the-art electrochemical and hybrid electrochemical-thermochemical processes for CH_4, MeOH and EtOH generation, and the corresponding system level STF conversion efficiency were then compared and contrasted to the thermochemical approaches. Target overpotentials and Faradaic efficiency (FE) for the electrochemical CO_2 reduction reactions was also presented to compete with thermochemical approaches at different operating scenarios.

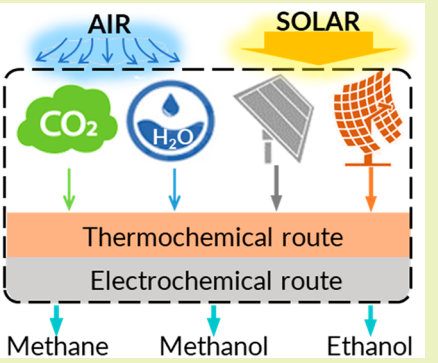

KEYWORDS: *Electrochemical CO_2 reduction, Thermochemical CO_2 reduction, Solar-to-fuel efficiency, Carbonaceous fuel, Direct air capture*

INTRODUCTION

Sunlight and air are the most abundant and accessible forms of energy and feedstock. To achieve the long-term global goal of carbon neutrality, a sunlight driven system that converts air into renewable fuels is highly desirable and highly resilient. Harnessing the energy from sunlight and using feedstocks from air to produce fuels and chemicals are no longer a far-fetched reality, thanks to the tremendous research advances in the area of photovoltaics,[1] solar-thermal conversion,[2,3] CO_2 and H_2O capture from air,[4−7] water electrolysis (EL),[8] and (photo)-electrochemical CO_2 conversion in recent years.[9,10] Carbonaceous fuels, especially for liquid fuels, such as methanol and ethanol, are highly value-add chemicals as well as cheap in storage and transportation. In comparison to artificial routes, fast-growing crops in nature have a sunlight conversion efficiency of ∼3% using CO_2 in air as the carbon feedstock.[11,12] For long duration energy storage and for enabling a sustainable future for society, abiotic approaches with higher efficiency, selectivity, and stability are highly desirable.[13] The solar driven electrochemical and thermochemical routes for carbonaceous fuel generation requires efficiency and cost-effective production of electrons or heat.

The generation of renewable electrons and holes from sunlight from photovoltaics have reached unprecedented efficiency for multijunction solar cells and low cost which further enables low-cost renewable fuel generation for crystalline silicon solar cells. A six-junction III−V solar cell with a world record 47.1% solar to electricity conversion efficiency under concentrated illumination was achieved.[14] At the same time, silicon solar cells with a lower conversion efficiency,[15] are still in vast commercial applications, especially at the utility scale, due to its competitive cost per kWh electricity generation.[1] For high temperature solar-thermal conversion (CST) systems, the receivers rely on a working fluid, such as molten salt, to restore and transport the heat energy converted from concentrated solar power. These technologies have been integrated to solar power plants and industrial processes for large scale implementation.[16,17] The solar-to-heat conversion efficiency varies with its operation temperature, structure, working fluid, and rate of work. For example, a 75 kW pool boiler receiver reached 90% solar thermal conversion efficiency at 800 °C operation temperature,[2] while the efficiency of another 150 kW gas-particle receiver reached around 50−90% for various incident solar energy intensities and particle flow rates.[18]

Various technological pathways have been developed for feedstock capture, for example, CO_2 and H_2O, from air. For

Received: June 1, 2022
Revised: October 4, 2022
Published: October 12, 2022

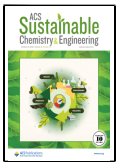

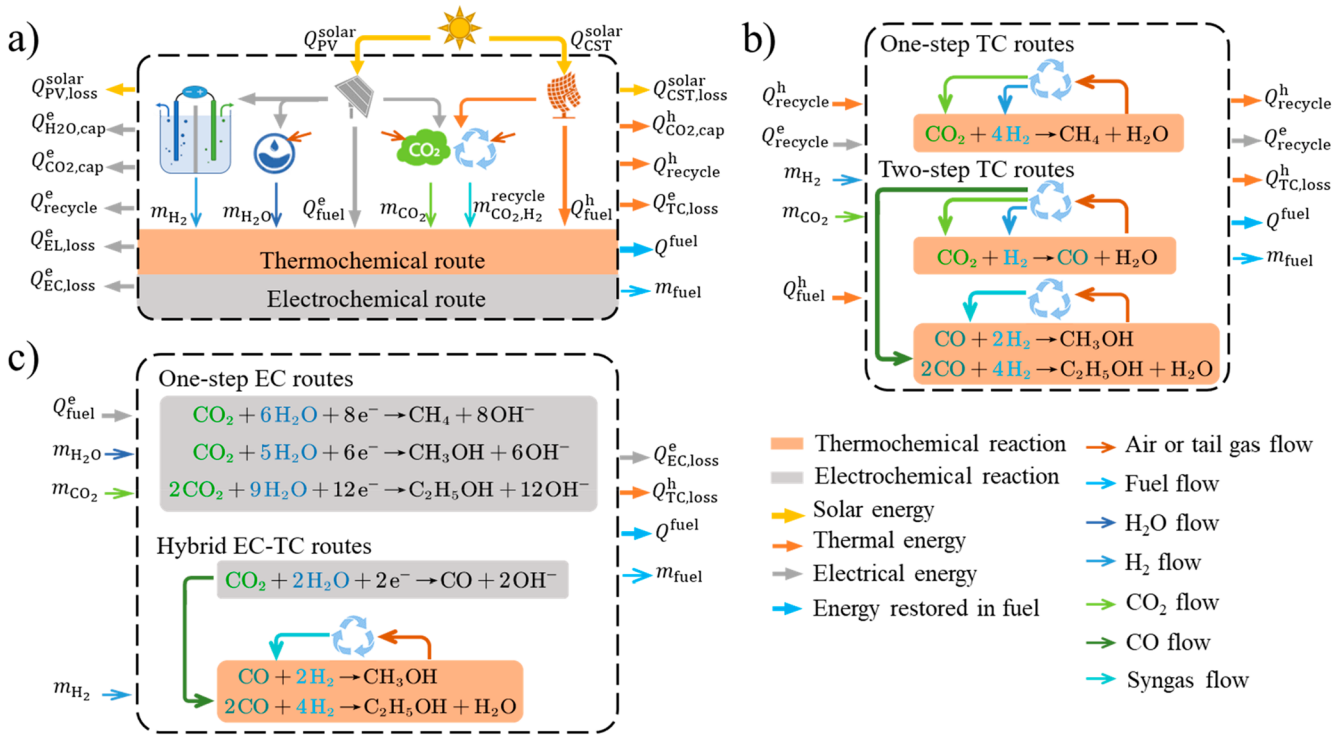

Figure 1. (a) Schematic illustration of all solar-driven thermochemical and electrochemical CO_2R routes including feedstock (CO_2 and H_2O) capture from air. (b) Thermochemical route for CH_4, MeOH, and EtOH formation. (c) Electrochemical route for CH_4, MeOH, and EtOH formation. The dash boxes are for CO_2R process. The orange-filled boxes represent the thermochemical route, and gray boxes represent the electrochemical routes.

direct CO_2 capture from air, the approaches, including solvent-based capture,[19−21] solid−sorbent-based capture,[22] and membrane-based capture,[23,24] have made significant progress in recent years. Direct air capture (DAC) is considered a promising technology for long-term global decarbonization.[25−27] The two most known DAC companies are Carbon Engineering and Climeworks, which pull the technology into large-scale implementation.[28−30] The DAC technology is not mature and is at an early commercial scale at the Technology Readiness Level (TRL) of 7−8 and whose largest direct air CO_2 capture capacity currently is about 1 ton CO_2/day.[31] For H_2O capture from air, several approaches have been explored. Membrane or mesh-based systems that capture water vapor from the atmosphere and collect water droplets via gravity have been reported in several studies and have achieved a scale of 2−6 ton/day.[32] The atmospheric water harvesting using the membrane or desiccant-assisted humidity-harvesting systems is at the TRL of 8−9.[31,33] Additionally, water can also be captured from air via radiative cooling, which relies on infrared emission properties of radiative emitters for to condense water vapor.[34,35]

In terms of the conversion processes, both electrochemical and thermochemical processes have the potential to produce cost competitive hydrocarbons. For water electrolysis, there has been a tremendous interest in green hydrogen in recent years, with low temperature electrolysis (LTE) as one of the most promising routes to deliver low cost and low emission H_2 via renewable electricity. The cost and efficiency of LTE have improved over the years, with MW to GW scale LTE systems being deployed worldwide.[36−39] For (photo)electrochemical CO_2 reduction (CO_2R), significant advances in selectivity, activity and durability of several multielectron and multiproton reactions have been recently made. For example, ethylene generation has reached an operating current density of 1.3 A cm^{-2} and a Faradaic efficiency (FE) of 65−75%,[40] and ethanol (EtOH) generation has reached a remarkable FE of 91% at −0.7 V versus RHE.[41] While the demonstrated scale for electrochemical approaches is limited to less than 1 kg/day, these electrochemical performance metrics have shown promise for potential commercialization of this technology.[42] In contrast, thermochemical CO_2 hydrogenation reactions have been well established and are used at industrial scale (million tons/year), including the Fischer−Tropsch process to produce fuels.[43] The Sabatier reaction is another example, which converts CO_2 and H_2 in a self-sustaining exothermic reaction to produce CH_4.[44] A 6 MW demonstration has been built and demonstrated terrestrially,[45] and there is a growing interest for scaling up this technology for space exploration.

While each technology has its own performance and efficiency metrics, the coupling of these technologies and the system level efficiency for the generation of fuels with the only energy input from sunlight and only air as a feedstock has not yet been reported. In particular, almost all electrochemical CO_2 reduction reports used pure CO_2 near 1 bar as the feedstock.[41] Hence, the reported solar-driven CO_2 reduction efficiency[40,41] is not directly comparable to photosynthetic processes, in which ~400 ppm of CO_2 in the presence of O_2 is used as the feedstock. In this study, we used sunlight and air as the only energy input and feedstock, respectively, and analyzed the overall system level solar-to-fuel (STF) conversion efficiency for CH_4, MeOH, and EtOH generation. In this comparative study, we benchmarked the system using state-of-the-art direct electrochemical conversion processes against the more traditional thermochemical reactions (TC) in which H_2

https://doi.org/10.1021/acssuschemeng.2c03230
ACS Sustainable Chem. Eng. 2022, 10, 13945−13954

was produced via water electrolysis. We aim to define the target FE and overpotentials for specific electrochemical fuel forming reactions required to compete with the traditional approaches.

MODELING

The model uses sunlight as the only energy input for the system which captures CO_2 and H_2O from air, and converts them into CH_4, MeOH, or EtOH via electrochemical CO_2R or thermochemical hydrogenation reactions (Figure 1a). The electrochemical reactions (EC) are highlighted in gray boxes, while the thermochemical hydrogenation reactions are highlighted in orange boxes. We considered a DAC process based on aqueous alkali solvent coupled with a calcium caustic loop.[30] The aqueous KOH solvent as the CO_2 sorbent with the calcium loop to regenerate the KOH solvent by adding $Ca(OH)_2$ to the system followed by a $CaCO_3$ sediment separation process. The calcium solvent ($Ca(OH)_2$) is then reproduced by $CaCO_3$ calcining and CaO hydrating. This process can operate continuously and allows industrial-level scaling economically. The reported energy consumption was 5.25 GJ of gas and 366 kWh of electricity per ton of CO_2 captured.[30] In this study we assume that the energy input required from the DAC process are provided by the thermal energy from a concentrated solar thermal (CST) device and the electricity from a photovoltaic (PV) device. This DAC process reported an energy utilization of $Q^{e}_{CO_2,0,}$ = 0.366 kWh $kg^{-1}_{CO_2}$ for electrical energy and $Q^{h}_{CO_2,0,}$ = 1.458 kWh $kg^{-1}_{CO_2}$ for thermal energy (equals to 5.25 GJ/t-CO_2) based on a large-scale plant techno-economic analysis.[30] For the H_2O capture process, we adapted an active cooling condensation process in which only electricity input from a PV device was required for H_2O capture and purification from air. The H_2O capture from air involves condensation and purification with the energy consumption estimated based on a commercialized project.[46] We assumed an ideal moisture content and relative humidity where the energy utilization efficiency was $Q^{e}_{H_2O,0}$ = 0.18 kWh $kg^{-1}_{H_2O}$ operating at ∼70−90% relative humidity and 22−35 °C ambient temperature.

The hydrogen was produced from water electrolyzer. The energy consumption for generating 1 kg of hydrogen via water electrolysis was assumed to be 55 kWh,[47] which was equivalent to an electricity-to-hydrogen efficiency of $\eta_{EL} = \Delta G^{0}_{H_2}/Q^{e}_{EL,0}$ = 59.9%. Apart from water electrolysis, the solar-driven thermochemical redox cycle can produce hydrogen from water utilizing metal oxide that participating the reduction and oxidation reactions sequentially and continuously.[48] It is reported that the highest possible STF efficiency is 36% from thermodynamic analysis,[49] while the highest lab-scale prototype efficiency is 5.25%[50] and the industrial-scale application efficiency is 4.1%.[51] Hence, we only considered this more matured solar hydrogen technologies instead of solar thermochemical hydrogen production pathway.

For all routes involving thermochemical reactions (Figure 1b), a feedstock recycling process was considered, including all TC pathways as well as the hybrid EC-TC routes in Figure 1c. For the reverse water gas shift reaction (rWGS) and CO hydrogenation reaction, we considered CO_2, CO and hydrogen recovery. For the CO hydrogenation reactions for the synthesis of MeOH and EtOH, the separation process was only a condensation process of MeOH and EtOH, where the leftover syngas could be fully recovered. Hence, the energy requirement for this separation step was negligible. For the removal and recycling of CO_2 from the syngas produced in rWGS for the two-step MeOH and EtOH formation route, we considered a conventional amine system with 100% CO_2 absorption and desorption efficiency. Further, the pressure swing adsorption (PSA) method was considered to recover hydrogen from the products of the rWGS reaction. The industrial PSA hydrogen separation can achieve a high purification level (99.999%) at Linde Engineering and Air Products PSA plants.[52,53] As a result, the utilization efficiencies of CO_2 and H_2 were assumed to be 100% from the single pass thermodynamic limitation of 57.9% (1 bar, 1050 °C) for rWGS reaction. The energy consumptions for the CO_2 and hydrogen recycling processes were $Q^{h}_{CO_2,recycle,0}$ = 0.3 kWh $kg^{-1}_{CO_2}$ for thermal energy and $Q^{e}_{H_2,recycle,0}$ = 1.13 kWh $kg^{-1}_{H_2}$ for electricity based on a large-scale plant techno-economic analysis.[54−56] All the device efficiencies and the energy consumption rates were summarized in Table S2.

For direct electrochemical CO_2R, the PV component was assumed to be operated at its maximum power point with a DC−DC converter to match the electrochemical load curves for CO_2R reactions, as well as for water splitting reactions. The number of electrons and equilibrium potentials of the electrochemical reactions involved in this comparison are listed in Table 1.

Table 1. Cathodic Electrochemical Reactions, Number of Electrons, and Cathodic Half Reactions' Equilibrium Potentials versus SHE[a]

fuel-forming reaction	N_e	E^{0}_{SHE} (V)
$2H^+ + 2e^- \rightarrow H_2$ (E-1)	2	0
$CO_2 + H_2O + 2e^- \rightarrow CO + 2OH^-$ (E-2)	2	−0.1
$CO_2 + 6H_2O + 8e^- \rightarrow CH_4 + 8OH^-$ (E-3)	8	0.17
$CO_2 + 5H_2O + 6e^- \rightarrow CH_3OH + 6OH^-$ (E-4)	6	0.03
$2CO_2 + 9H_2O + 12e^- \rightarrow C_2H_5OH + 12OH^-$ (E-5)	12	0.08

[a]Note that the equilibrium potential for anodic half reaction vs SHE is 1.23 V.

For the thermochemical hydrogenation reactions, the feedstock hydrogen was produced via electrochemical water splitting process powered by PV and the feedstock CO_2 was collected from DAC process. Their reaction equations and entropy changes from literature reported operation conditions are listed in Table 2. Thermodynamic carbon conversion ratios of the involved reactions as the function of pressure and temperautre were concluded in Figure S1. Among the reactions the rWGS reaction is endothermic, the entropy changes of which were compensated by the heat energy generated from concentrated solar thermal device. The remaining reactions are exothermic, where zero additional heat input was assumed under the equilibrium condition with reasonable insulation. For thermochemical reactions (orange boxes in Figure 1), the Sabatier reaction was considered for CH_4 production. Due to its energy downhill nature, the reaction can operate in a self-sustainable manner without additional energy input for continuous reaction. In addition, the Sabatier reaction has favorable thermodynamics (carbon utilization efficiency of 94.9%) at typical operation condition (1 bar, 300 °C), and recycling is also considered. For MeOH

https://doi.org/10.1021/acssuschemeng.2c03230
ACS Sustainable Chem. Eng. 2022, 10, 13945−13954

Table 2. Thermochemical Reaction Equations, And Their Reaction Enthalpy Changes, ΔH, and Carbon Utilization Efficiency, $\chi^{TC}_{CO_2}$, at Stoichiometric Feedstock Ratio under Typical Industrial Operation Conditions

thermochemical reaction equation	$\chi^{TC}_{CO_2}$
one-step CH_4 (one-step TC)	
$CO_2 + 4H_2 \rightarrow CH_4 + 2H_2O(g)$, $\Delta H = -177.2$ kJ mol^{-1} (T-1)	94.9% (1 bar, 300 °C)[58,59]
two-step MeOH (two-step TC)	
$CO_2 + H_2 \rightarrow CO + H_2O(g)$, $\Delta H = 31.7$ kJ mol^{-1} (T-2.1)	57.9% (1 bar, 1050 °C)[60]
$CO + 2H_2 \rightarrow CH_3OH(g)$, $\Delta H = -98.4$ kJ mol^{-1} (T-2.2)	47.5% (50 bar, 260 °C)[61]
two-step EtOH (two-step TC)	
$CO_2 + H_2 \rightarrow CO + H_2O(g)$, $\Delta H = 31.7$ kJ mol^{-1} (T-3.1)	57.9% (1 bar, 1050 °C)[60]
$2CO + 4H_2 \rightarrow C_2H_5OH(g) + H_2O(g)$, $\Delta H = -135.2$ kJ mol^{-1} (T-3.2)	73.7% (50 bar, 300 °C)[62]

and EtOH production, the two-step TC routes were studied. The production was achieved by a two-step hydrogenation chain reaction.

For the electricity generation, crystalline silicon PV cells with a 23% solar-to-electricity conversion efficiency, η_{PV}, was used in the calculation, which represented a typical value of industrially manufactured solar cells.[57] For the heat generation, an 80% photothermal conversion efficiency, η_{CST}, was considered.[2] Heat was used to power the steam heating unit for the CO_2 capture module and to balance the endothermic enthalpy change of the rWGS for the thermochemical route in Figure 1a,b.

THERMOCHEMICAL ROUTE ENERGY BALANCE ANALYSIS

Figure 2a shows the energy requirements (kWh kg^{-1} of fuel) for generating fuels via three thermochemical approaches. The

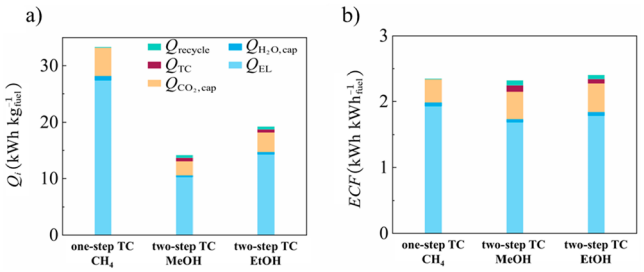

Figure 2. Energy requirements in terms of (a) kWh kg^{-1} of fuel or (b) kWh kWh^{-1} of fuel for generating fuels via thermochemical approaches. The required total energy via thermochemical approaches includes energy consumption for CO_2 capture and H_2O capture, $Q_{CO_2,cap}$ and $Q_{H_2O,cap}$, recycle, $Q_{recycle}$, thermochemical reaction, Q_{TC}, and water electrolysis, Q_{EL}.

total required energy is categorized into solar energy converted by PV and CST to provide electricity and thermal energy which are consumed by CO_2 and H_2O capture and recycle processes, as well as fuel generation related processes. The detail definitions for all energy terms can be found in modeling section.

As shown in Figure 2a, since water electrolysis, Q_{EL}, is the dominant energy demand in all the thermochemical approaches, an efficient utilization of H_2 becomes very important to achieve high STF energy conversion efficiency. CH_4 has the highest heat content among all the fuels considered in this study, and as a result, CH_4 generation via the Sabatier reaction (one-step TC CH_4) exhibited the highest required energy input per kg of fuel, that is, 33.29 kWh kg^{-1}. The two-step TC MeOH generation route exhibited the lowest energy requirements 14.12 kWh kg^{-1} due to the low heat content of MeOH.

Note that the energy requirement for recycling of CO_2 and H_2 are also shown in Figure 2a. The one-step TC CH_4 route exhibited the lowest energy requirement for recycling, 0.0716 kWh kg^{-1}, due to its high single pass CO_2 conversion. The feedstock recycle energy consumption for the three routes is also calculated by minimum separation power of a separation process (MSPS) in Figure S2, which is listed and compared with the values calculated from literature reported data in Table S3.

Both the two-step TC EtOH and MeOH generation routes have a common first thermochemical step, for example, rWGS, and the two-step EtOH generation exhibited a larger kWh kg^{-1} value than the two-step MeOH generation due to the larger water electrolysis energy requirement for EtOH.

Figure 2b compares the total amount of energy requiremened in kWh to produce 1 kWh fuel in Gibbs free energy among the three routes. The energy requirements include electricity energy inputs for feedstock capture, recycle and powering water electrolysis, as well as heat energy inputs for endothermic thermochemical reactions, feedstock capture and recycle. We defined the term, Energy consumption factor (ECF), to describe the energy requirements per kWh fuel generating. All three routes showed a similar energy requirement, 2.34 kWh kWh$_{fuel}^{-1}$ for CH_4, 2.32 kWh kWh$_{fuel}^{-1}$ for MeOH, and 2.40 kWh kWh$_{fuel}^{-1}$ for EtOH.

The system-level STF conversion efficiency in this study considered both the energy conversion and feedstock capture processes, such as the solar-to-electricity conversion in PV and thermochemcial reaction, and the feedstock capture process from dilute sources, such as CO_2 capture from air. The system-level STF conversion efficiency, as shown in Figure 3. $\eta_{PV,loss}$ was the dominating energy component for all three routes (see light blue bars in Figure 3) and account for 68.9% for one-step TC CH_4, 64.6% for two-step TC MeOH, and 65.5% for two-step TC EtOH. This was due to the limited solar-to-electricity conversion efficiency of 23% considered in this study. The MeOH generation route showed the highest STF efficiency of 11.4%, while CH_4 generation showed the lowest STF effiency of 10.7%. This is consistent with the ECF values in Figure 2b. The optimum overall STF conversion efficiency of the two-step TC MeOH formation reactions was off the stoichiometric ratio calculated from thermodynamic reaction conversion

https://doi.org/10.1021/acssuschemeng.2c03230
ACS Sustainable Chem. Eng. 2022, 10, 13945−13954

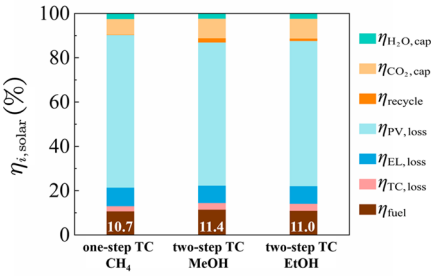

Figure 3. System level STF conversion efficiencies for three thermochemical fuel forming approaches. The solar energy consumption was categorized into feedstock capture process and STF energy conversion process, according to the energy conversion processes shown in Figure 1a. The former includes energy consumption for H_2O and CO_2 capture, $\eta_{H_2O,cap}$, $\eta_{CO_2,cap}$, and feedstock recycle, $\eta_{recycle}$. The energy conversion consisted of PV loss, $\eta_{PV,loss}$, electrolyzer loss, $\eta_{EL,loss}$, thermochemical reaction loss, $\eta_{TC,loss}$, and energy stored in fuel, η_{fuel}.

limits shown in Figure S3. It is interesting that the excess CO_2 supply helps increase STF efficiency due to high ulitzation efficiency of hydrogen at higher CO_2 fractions in the reactants.

ELECTROCHEMICAL AND THERMOCHEMICAL ROUTE COMPARISON

The comparison of the system level STF conversion efficiencies between the reported electrochemical and the calculated thermochemical CH_4 generation routes is shown in Figure 4. The one-step EC CH_4 generation route involved eight electrons and eight protons per carbon (reaction E-3 in Table 1). Figure 4 shows the system-level STF conversion efficiency as a function of the overpotential for CO_2R and the FE for CH_4 generation reaction. The STF conversion efficiency of the corresponding solar driven thermochemical approach, and the reported electrochemical CO_2R performance (Table 3) were plotted as a red dash line and colored dots, respectively. The electrode potential calculation procedures are shown in Table S4.

As shown in Figure 4, all the reported electrochemical performance values for CH_4 generation clustered far below the STF conversion efficiency from the thermochemical pathway of 10.7%. The low STF conversion efficiency of the electrochemical pathway was due to the large kinetic overpotentials and low FE. In addition, many reported CO_2R materials for CH_4 generation have operated far below the operating current density that is relevant for solar-driven processes (tens of mA cm^{-2}). To achieve materials performance at higher operating current density with a much lower overpotential and much higher FE would require significant research advances in the future.

To compete with the thermochemical pathway, significant advances in catalyst performance are required. For example, an overpotential of −0.63 V and a FE of 100% or an overpotential of −0.1 V and a FE of 74% is required to achieve the same STF conversion efficiency of the thermochemical process. In addition, an ideal (100%) single pass carbon utilization efficiency for the electrochemical conversion process was assumed inFigure 5. Lower carbon utilization efficiency or the use of multipass electrochemical cells that would require additional gas separation process would further decrease the system level STF conversion efficiency for the electrochemical route for CH_4 generation. A lower carbon utilization efficiency in the electrochemical approach would also be very sensitive to the energy requirements for the CO_2 capture process. Furthermore, the competing hydrogen evolution reaction (HER) and other electrochemical CO_2R reactions with similar reduction potentials would present significant challenges for near unity FE for CH_4 generation.[82−84] Hence, from the energy balance point of view, the thermochemical process is much more favorable than the electrochemical route. The energy breakdowns for the five CH_4 catalysts are compared in Figure 4b. $\eta_{PV,loss}$ took the major energy consumption, followed by the $\eta_{EC,loss}$. $\eta_{EC,loss}$ is dictated by the catalysts' performance, which leads to the highest η_{STF,CH_4} of 9.87% achieved by using the cathode catalyst reported by Pan et al.[66] The energy breakdowns for other electrochemical routes are compared in Figure S5.

In contrast, as shown in Figure 5a,b, there were several reported electrochemical CO_2R systems for MeOH generation with higher STF conversion efficiency than their corresponding thermochemical approaches. The two best electrochemical STF efficiencies were estimated to be 12.24% and 12.41% for the one-step EC route and hybrid EC-TC route for MeOH

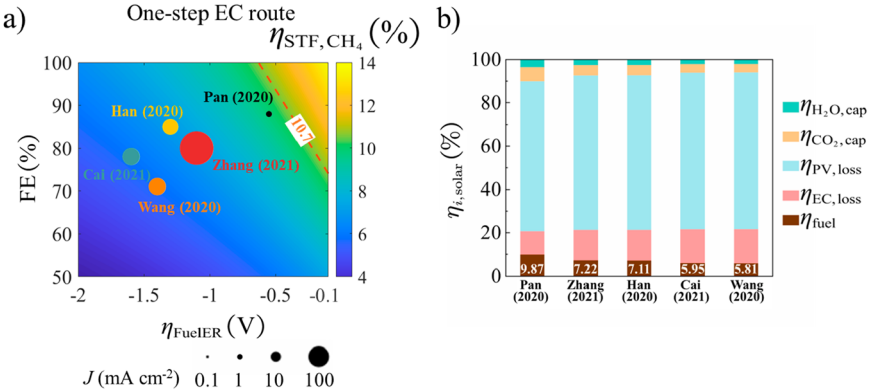

Figure 4. (a) System level STF conversion efficiency as a function of the overpotential for electrochemical CO_2R at the cathode and the FE for CH_4 electrochemical forming reaction. The STF conversion efficiency of the corresponding solar driven thermochemical approach, and the reported electrochemical CO_2R performance are plotted as a red dash line and colored dots, respectively. The size of the dots represents the reported current densities at the given overpotentials. (b) STF conversion efficiencies for five CH_4 generation catalysts. The energy consuption was broken down into H_2O and CO_2 capture, $\eta_{H_2O,cap}$, and $\eta_{CO_2,cap}$, PV loss, $\eta_{PV,loss}$, electrochemical reaction loss, $\eta_{EC,loss}$, and energy stored in fuel, η_{fuel}.

https://doi.org/10.1021/acssuschemeng.2c03230
ACS Sustainable Chem. Eng. 2022, 10, 13945−13954

Table 3. FE, Overpotential, Current Density, and Material of the Reported Electrochemical CO_2R Electrode

final product	author	FE	F_{fuelER}[a]	η_{fuelER}	J ($mAcm^{-2}$	material[b]	ref
CH_4	Cai (2021)	0.78	$-1.44V_{RHE}$(0.5 M $KHCO_3$)	−1.6	40	Cu MNCs	63
	Wang (2020)	0.71	$-1.20V_{RHE}$(0.5 M $KHCO_3$)	−1.4	37	Cu−Bi NPs	64
	Han (2020)	0.85	$-1.80V_{SCE}$(1 M $KHCO_3$)	−1.3	31.8	SA-Zn MNCs	65
	Pan (2020)	0.88	$-0.38V_{RHE}$(0.1 M $NaHCO_3$)	−0.55	0.31	Cu/Nafion	66
	Zhang (2021)	0.80	$-0.90V_{RHE}$(1 M KOH)	−1.1	203	Cu/Cu_2O MNCs	67
MeOH	Huang (2018)	0.97	$-0.98V_{SCE}$(0.1 M $NaHCO_3$)	−0.36	0.59	$Co(CO_3)_{0.5}OH{\cdot}11H_2O$	68
	Yang (2019)	0.78		−0.29	41.5	$Cu_{2-x}Se(y)$ NPs	69
	Mou (2019)	0.92	$-0.50V_{RHE}$(0.1 m $KHCO_3$)	−0.53	0.2	boron phosphide NPs	70
	Periasamy (2018)	0.93	$-0.85V_{RHE}$(0.5 M $KHCO_3$)	−0.88	0.25	Cu_2O NPs	71
	Lu (2018)	0.80		−0.24	31.8	Pd−Cu AG	72
CO	Geng (2017)	0.83	$-1.10V_{RHE}$(0.1 M $KHCO_3$)	−1.0	16.1	ZnO NSs	73
	Möller (2019)	0.85	$-1.00V_{RHE}$(1 M $KHCO_3$)	−0.90	200	Ni MSCs	74
	Jiao (2019)	0.92	$-0.78V_{RHE}$(0.2 M $NaHCO_3$)	−0.68	8.6	Cu-doped $Pd_{10}Te_3$ NWs	75
	Zhang (2019)	0.97	$-0.46V_{RHE}$(0.1 M $KHCO_3$)	−0.36	1.9	FeN_5 MNCs	76
	Nellaiappan (2020)	1.00	$-0.30V_{RHE}$(0.5 M K_2SO_4)	−0.20	13.8	AuAgPtPdC NPs	77
EtOH	Xu (2020)	0.91	$-0.70V_{RHE}$(0.1 M $KHCO_3$)	−0.78	5	Cu/C NPs	41
	Zhang (2020)	0.71	$-0.87V_{RHE}$(0.5 M $KHCO_3$)	−0.95	10.4	Cu/Cu_2O MNCs	78
	Yuan (2019)	0.56	$-0.25V_{RHE}$(0.1 M $KHCO_3$)	−0.33	4.7	Cu/C NPs	79
	Lv (2018)	0.85	$-0.60V_{RHE}$(0.1 M $KHCO_3$)	−0.68	0.35	Ag MNCs	80
	Wang (2020)	0.52	$-0.68V_{RHE}$(0.1 M $KHCO_3$)	−0.76	156	Cu MNCs	81

[a]CO_2 saturated 0.1 M $KHCO_3$ pH = 6.8,[80] 0.5 M $KHCO_3$ pH = 7.33,[78] 1 M $KHCO_3$ pH = 7.7,[74] 1 M KOH pH = 13.9,[81] 0.2 M $NaHCO_3$ pH = 7.[75] [b]NP = nanoparticle; NC = nanocrystal; NW = nanowire; NS = nanosheet; SA = single atom; MNC = microporous nitrogen-doped carbon; AG = aerogel; Note that the detailed calculation procedure for potential conversions is from eqns S7−S11.

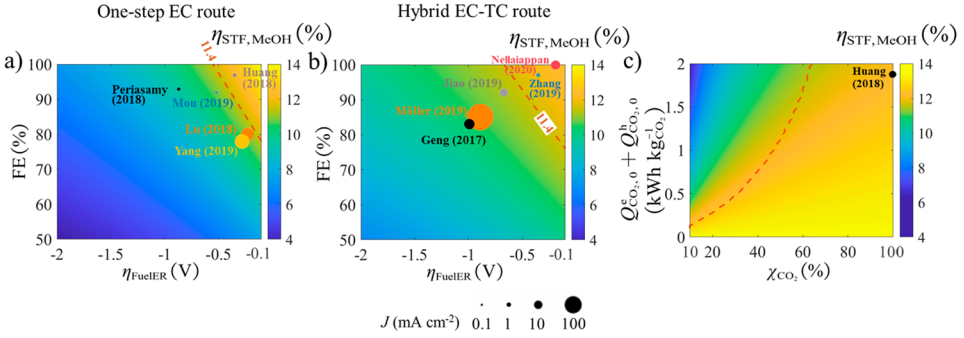

Figure 5. (a) System level STF conversion efficiency as a function of the overpotential for electrochemical CO_2R at the cathode and the FE for one-step EC route and (b) hybrid EC-TC route for MeOH forming. The STF conversion efficiency of the corresponding solar driven thermochemical approaches, and the reported electrochemical CO_2R performance are plotted as red dash line and colored dots, respectively. The size of the dots represents the reported current densities at the given overpotentials. (c) STF efficiency as the function of CO_2 utilization efficiency and CO_2 capture energy consumption of the electrochemical CO_2R case reported by Huang[68] which belongs to the one-step EC route. The STF efficiencies of the one-step TC route with 0−2 kWh kg^{-1} CO_2 capture energy consumption was plotted in the dash line.

formation respectively. The electrochemical, hybrid EC-TC route involved an electrochemical CO generation process and a subsequent thermochemical hydrogenation process for MeOH generation. The higher STF efficiency in the hybrid EC-TC MeOH route was due to the efficient electrochemical CO generation from CO_2. An alternative electrochemical, two-step MeOH formation route was depicted in Figure S6, in which syngas was generated from a single-electrolysis cell by the simultaneous reduction of CO_2 and H_2O at the ratio of 1:2. The reported materials had high FE but large overpotential, so the system-level STF efficiency was lower than the thermochemical routes.

Figure 5c shows the impact of CO_2 utilization efficiency and CO_2 capture energy requirement on the system level STF conversion efficiency of an one-step EC MeOH generation process with an overpotential of −0.36 V and a FE of 97%.[68] The STF conversion efficiency shows a minimal value of about 6.3% at 10% CO_2 utilization efficiency with $Q^e_{CO_2,0} + Q^h_{CO_2,0}$ = 2 kWh $kg^{-1}_{CO_2}$, and a peak value of about 13.5% at 100% CO_2 utilization efficiency with $Q^e_{CO_2,0} + Q^h_{CO_2,0}$ = 0 kWh $kg^{-1}_{CO_2}$. The red dashed line in Figure 5c is the STF conversion efficiency of the two-step TC MeOH route with changing CO_2 capture energy consumption. When $Q^0_{CO_2,0}$ = 0.13 kWh $kg^{-1}_{CO_2}$, the STF efficiency is close to 12.5%. This value reduced to 11.4% when $Q^0_{CO_2}$ increased to 2 kWh $kg^{-1}_{CO_2}$. The left side of the dash line indicates a better performing thermochemical route, while on the right ride, the electrochemical route outperforms.

It is interesting to note that the electrochemical process can tolerate rather low CO_2 utilization efficiency, especially if the energy requirement for the CO_2 capture process is low. For example, the CO_2 utilization efficiency only needs to be greater than about 31% at a $Q^e_{CO_2,0} + Q^h_{CO_2,0}$ = 0.5 kWh $kg^{-1}_{CO_2}$ to achieve a competitive STF conversion efficiency relative to the

https://doi.org/10.1021/acssuschemeng.2c03230
ACS Sustainable Chem. Eng. 2022, 10, 13945−13954

thermochemical approaches. In addition, when the $Q^{e}_{CO_2,0}$ + $Q^{h}_{CO_2,0}$ was lower than 0.13 kWh $kg^{-1}_{CO_2}$, the electrochemical route exhibited a higher STF efficiency than the thermochemical approach, because the system level STF efficiency was no longer sensitive to CO_2 capture energy consumption. The STF efficiency as the function of CO_2 utilization efficiency and CO_2 capture energy consumption of the reported electrochemical CO_2R cases of other fuel formation routes were depicted in Figure S7. The electrochemical catalysts for CO generation show high FE and high current density in Table 3. As shown in Figure S8, the thermochemical and electrochemical routes are in similar efficiency ranges for CO production.

The direct electrochemical conversion of CO_2 to EtOH involves 12 electrons and 12 protons transferred per mole of EtOH (reaction E-5, Table 1). Significant advances have been made in the electrochemical conversion of CO_2 to EtOH. For example, the highest EtOH evolution FE achieved so far is 91%,[41] while another reported catalyst performed at 156 mA cm^{-2} EtOH conversion current density.[81] As shown in Figure 6a, the comparisons of thermochemical and one-step electrochemical CO_2R for EtOH generation are similar to those of CH_4 generation in Figure 4. All the reported electrochemical materials and devices shows a lower STF conversion efficiency than the thermochemical approach with recycling, even with assuming unity carbon utilization efficiency. For example, to compete with thermochemical approaches with recycling, an overpotential of −0.55 V and a FE of 78% is required for one-step EC route, and another overpotential of −0.58 V and a FE of 77% is required for the hybrid two-step EC route EtOH generation.

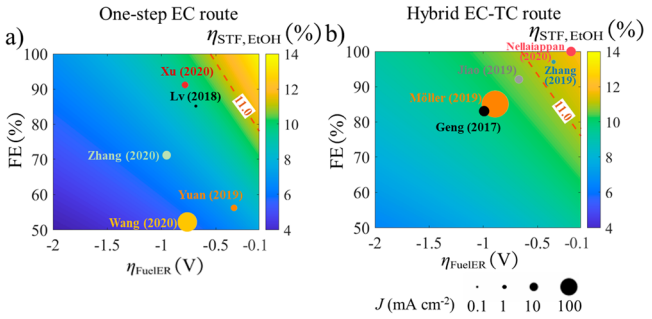

Figure 6. System level STF conversion efficiency as a function of the overpotential for electrochemical CO_2R at the cathode and the FE for EtOH electrochemical forming reaction: (a) one-step EC route and (b) hybrid EC-TC route. The STF conversion efficiency of each solar driven thermochemical approach and the reported electrochemical CO_2R performance are plotted as red dash line and colored dots, respectively. The size of the dots represents the reported current densities at the given overpotentials.

We used 10 mA cm^{-2} as our reference value because most nonconcentrated solar-driven (photo)electrochemical CO_2 reduction devices operate at similar current densities. However, for future industrial/application relevant operations, 100 mA cm^{-2} or even higher values should be considered. Therefore, we have added additional calculations in Figure S9 for 100 mA cm^{-2} cases showing that the electrochemical performance was reduced due to the increased overpotentials at higher operating current densities.

CONCLUSIONS

For thermochemical approaches, the overall energy requirements in kWh to produce 1 kWh of fuels in Gibbs free energy ranged from 2.3 to 2.4 kWh kWh^{-1}_{fuel} for CH_4, MeOH, EtOH generation with recycling, using sunlight as the only energy input and air as the only feedstock. The energy requirements for water electrolysis for H_2 generation dominated the overall energy demand in all the thermochemical approaches, and as a result, high H_2 utilization efficiency by recycling becomes important to achieve high system level STF conversion efficiency. The energy requirement for H_2O and CO_2 capture make up small portions in the overall STF conversion process.

For the electrochemical approaches to be competitive with the thermochemical approaches, significant advances in reducing the overpotential and increasing the FE for CO_2 reduction reaction are required. Presently, in terms of the overall STF conversion efficiency, the electrochemical CH_4 generation has the largest gap relative to the thermochemical approaches, while the electrochemical MeOH generation already have materials and devices with performance metrics that can compete with thermochemical approaches.

Since the energy requirement for CO_2 capture is much less than the electrochemical CO_2 conversion process, low CO_2 utilization efficiencies can still lead to a relatively high overall system efficiency in the electrochemical approaches. As an example, for MeOH generation the CO_2 utilization efficiency only needs to be greater than 64% at a CO_2 capture energy requirement of 2 kWh kg^{-1} to achieve a competitive STF conversion efficiency relative to the thermochemical approaches.

ASSOCIATED CONTENT

Supporting Information

The Supporting Information is available free of charge at https://pubs.acs.org/doi/10.1021/acssuschemeng.2c03230.

Computational methods; Data used in simulation models; Effects of CO_2 utilization efficiency and CO_2 capture energy consumption; System level STF efficiency of two-step MeOH route changing with feedstock ratio; Comparison of thermochemical and electrochemical routes for CO formation; System level STF conversion efficiency at 100 mA cm^{-2} current density (PDF)

AUTHOR INFORMATION

Corresponding Authors

Chengxiang Xiang − *Liquid Sunlight Alliance, Department of Applied Physics and Material Science, California Institute of Technology, Pasadena, California 91125, United States;* orcid.org/0000-0002-1698-6754; Email: cxx@caltech.edu

Meng Lin − *Department of Mechanical and Energy Engineering, Southern University of Science and Technology, Shenzhen 518055, China;* orcid.org/0000-0001-7785-749X; Email: linm@sustech.edu.cn

Authors

Da Xu − *Department of Mechanical and Energy Engineering, Southern University of Science and Technology, Shenzhen 518055, China*

Ian Sullivan − *Liquid Sunlight Alliance, Department of Applied Physics and Material Science, California Institute of*

https://doi.org/10.1021/acssuschemeng.2c03230
ACS Sustainable Chem. Eng. 2022, 10, 13945−13954

Technology, Pasadena, California 91125, United States;
orcid.org/0000-0003-0632-4607

Complete contact information is available at:
https://pubs.acs.org/10.1021/acssuschemeng.2c03230

Notes

The authors declare no competing financial interest.

■ ACKNOWLEDGMENTS

This material is based on work performed by the Liquid Sunlight Alliance, which is supported by the U.S. Department of Energy, Office of Science, Office of Basic Energy Sciences, and Fuels from Sunlight Hub under Award Number DE-SC0021266. M.L. and D.X. acknowledge the support by the National Natural Science Foundation of China under Grant No. 52006097. The computation in this work is supported by Center for Computational Science and Engineering at Southern University of Science and Technology.

■ NOMENCLATURE

Abbreviations

CST concentrated solar thermal device
CO_2R (photo)electrochemical CO_2 reduction
DAC direct air capture
EC electrochemical reaction
ECF energy consumption factor
EL water electrolysis
EtOH ethanol
FE faradic efficiency
HER hydrogen evolution reaction
LTE low temperature electrolysis
MeOH methanol
MSPS minimum separation power of a separation process
OER oxygen evolution reaction
PSA Pressure swing adsorption
PV photovoltaic
rWGS reverse water gas shift reaction
STF solar-to-fuel
TC thermochemical reaction

Latin symbols

E electrode equilibrium potential (V)
ECF energy consumption factor (kWh kWh_{fuel}^{-1})
FE Faradaic efficiency (1)
J current density (mA cm^{-2})
m substance mass (kg)
N_e number of electrons transferred (1)
Q energy consumption (kW h)

Greek symbols

$\Delta G^0_{H_2}$ fuel Gibbs free energy (kWh kg^{-1})
ΔH reaction enthalpy change (kJ mol^{-1})
η efficiency (1), overpotential (V)
χ feedstock utilization efficiency (1)

Subscript

0 energy consumption per kilogram substance
cap feedstock capture
fuelER fuel evolution reaction
loss energy loss
ohmic ohmic potential
OER oxygen evolution reaction
recycle feedstock and product

Superscript

e electricity
h heat
solar equivalent solar energy

■ REFERENCES

(1) Victoria, M.; Haegel, N.; Peters, I. M.; Sinton, R.; Jäger-Waldau, A.; del Cañizo, C.; Breyer, C.; Stocks, M.; Blakers, A.; Kaizuka, I.; Komoto, K.; Smets, A. Solar Photovoltaics Is Ready to Power a Sustainable Future. *Joule* **2021**, *5* (5), 1041−1056.
(2) Lipiński, W.; Abbasi-Shavazi, E.; Chen, J.; Coventry, J.; Hangi, M.; Iyer, S.; Kumar, A.; Li, L.; Li, S.; Pye, J.; Torres, J. F.; Wang, B.; Wang, Y.; Wheeler, V. M. Progress in Heat Transfer Research for High-Temperature Solar Thermal Applications. *Applied Thermal Engineering* **2020**, 116137.
(3) Ravi Kumar, K.; Krishna Chaitanya, N. V. V.; Sendhil Kumar, N. Solar Thermal Energy Technologies and Its Applications for Process Heating and Power Generation - A Review. *Journal of Cleaner Production* **2021**, *282*, 125296.
(4) Sabatino, F.; Grimm, A.; Gallucci, F.; van Sint Annaland, M.; Kramer, G. J.; Gazzani, M. A Comparative Energy and Costs Assessment and Optimization for Direct Air Capture Technologies. *Joule* **2021**, *5* (8), 2047−2076.
(5) Erans, M.; Sanz-Pérez, E. S.; Hanak, D. P.; Clulow, Z.; Reiner, D. M.; Mutch, G. A. Direct Air Capture: Process Technology, Techno-Economic and Socio-Political Challenges. *Energy and Environmental Science.* **2022**, *15*, 1360−1405.
(6) Tu, Y.; Wang, R.; Zhang, Y.; Wang, J. Progress and Expectation of Atmospheric Water Harvesting. *Joule* **2018**, *2* (8), 1452−1475.
(7) Kandeal, A. W.; Joseph, A.; Elsharkawy, M.; Elkadeem, M. R.; Hamada, M. A.; Khalil, A.; Eid Moustapha, M.; Sharshir, S. W. Research Progress on Recent Technologies of Water Harvesting from Atmospheric Air: A Detailed Review. *Sustainable Energy Technologies and Assessments* **2022**, *52* (PA), 102000.
(8) Buttler, A.; Spliethoff, H. Current Status of Water Electrolysis for Energy Storage, Grid Balancing and Sector Coupling via Power-to-Gas and Power-to-Liquids: A Review. *Renewable and Sustainable Energy Reviews* **2018**, *82* (September 2017), 2440−2454.
(9) Wakerley, D.; Lamaison, S.; Wicks, J.; Clemens, A.; Feaster, J.; Corral, D.; Jaffer, S. A.; Sarkar, A.; Fontecave, M.; Duoss, E. B.; Baker, S.; Sargent, E. H.; Jaramillo, T. F.; Hahn, C. Gas Diffusion Electrodes, Reactor Designs and Key Metrics of Low-Temperature CO2 Electrolysers. *Nature Energy* **2022**, *7* (2), 130−143.
(10) Cheng, Y.; Hou, P.; Wang, X.; Kang, P. CO_2 Electrolysis System under Industrially Relevant Conditions. *Acc. Chem. Res.* **2022**, *55* (3), 231−240.
(11) Zhu, X. G.; Long, S. P.; Ort, D. R. Improving Photosynthetic Efficiency for Greater Yield. *Annual Review of Plant Biology* **2010**, *61*, 235−261.
(12) Zhu, X. G.; Long, S. P.; Ort, D. R. What Is the Maximum Efficiency with Which Photosynthesis Can Convert Solar Energy into Biomass? *Curr. Opin. Biotechnol.* **2008**, *19*, 153−159.
(13) Wang, F.; Harindintwali, J. D.; Yuan, Z.; Wang, M.; Wang, F.; Li, S.; Yin, Z.; Huang, L.; Fu, Y.; Li, L.; Chang, S. X.; Zhang, L.; Rinklebe, J.; Yuan, Z.; Zhu, Q.; Xiang, L.; Tsang, D. C. W.; Xu, L.; Jiang, X.; Liu, J.; Wei, N.; Kästner, M.; Zou, Y.; Ok, Y. S.; Shen, J.; Peng, D.; Zhang, W.; Barceló, D.; Zhou, Y.; Bai, Z.; Li, B.; Zhang, B.; Wei, K.; Cao, H.; Tan, Z.; Zhao, L. bin; He, X.; Zheng, J.; Bolan, N.; Liu, X.; Huang, C.; Dietmann, S.; Luo, M.; Sun, N.; Gong, J.; Gong, Y.; Brahushi, F.; Zhang, T.; Xiao, C.; Li, X.; Chen, W.; Jiao, N.; Lehmann, J.; Zhu, Y. G.; Jin, H.; Schäffer, A.; Tiedje, J. M.; Chen, J. M. Technologies and Perspectives for Achieving Carbon Neutrality. *Innovation* **2021**, *2* (4), na.
(14) Geisz, J. F.; France, R. M.; Schulte, K. L.; Steiner, M. A.; Norman, A. G.; Guthrey, H. L.; Young, M. R.; Song, T.; Moriarty, T. Six-Junction III-V Solar Cells with 47.1% Conversion Efficiency under 143 Suns Concentration. *Nature Energy* **2020**, *5* (4), 326−335.

(15) Battaglia, C.; Cuevas, A.; de Wolf, S. High-Efficiency Crystalline Silicon Solar Cells: Status and Perspectives. *Energy and Environmental Science. Royal Society of Chemistry* **2016**, *9*, 1552−1576.
(16) Merchán, R. P.; Santos, M. J.; Medina, A.; Calvo Hernández, A. High Temperature Central Tower Plants for Concentrated Solar Power: 2021 Overview. *Renewable and Sustainable Energy Reviews* **2022**, *155*, 111828.
(17) Kuravi, S.; Trahan, J.; Goswami, D. Y.; Rahman, M. M.; Stefanakos, E. K. Thermal Energy Storage Technologies and Systems for Concentrating Solar Power Plants. *Prog. Energy Combust. Sci.* **2013**, *39* (4), 285−319.
(18) Perez Lopez, I.; Benoit, H.; Gauthier, D.; Sans, J. L.; Guillot, E.; Mazza, G.; Flamant, G. On-Sun Operation of a 150 KWth Pilot Solar Receiver Using Dense Particle Suspension as Heat Transfer Fluid. *Sol. Energy* **2016**, *137*, 463−476.
(19) Barzagli, F.; Giorgi, C.; Mani, F.; Peruzzini, M. Screening Study of Different Amine-Based Solutions as Sorbents for Direct CO_2 Capture from Air. *ACS Sustainable Chem. Eng.* **2020**, *8* (37), 14013−14021.
(20) Yamada, H. Amine-Based Capture of CO2 for Utilization and Storage. *Polym. J.* **2021**, *53* (1), 93−102.
(21) Custelcean, R. Direct Air Capture of CO_2 Using Solvents. *Annu. Rev. Chem. Biomol. Eng.* **2022**, *13* (1), 217−234.
(22) Dunstan, M. T.; Donat, F.; Bork, A. H.; Grey, C. P.; Müller, C. R. CO_2 Capture at Medium to High Temperature Using Solid Oxide-Based Sorbents: Fundamental Aspects, Mechanistic Insights, and Recent Advances. *Chem. Rev.* **2021**, *121* (20), 12681−12745.
(23) Fujikawa, S.; Selyanchyn, R. Direct Air Capture by Membranes. *MRS Bull.* **2022**, *47* (4), 416.
(24) Castro-Muñoz, R.; Zamidi Ahmad, M.; Malankowska, M.; Coronas, J. A New Relevant Membrane Application: CO2 Direct Air Capture (DAC). *Chemical Engineering Journal* **2022**, *446*, 137047.
(25) Hanna, R.; Abdulla, A.; Xu, Y.; Victor, D. G. Emergency Deployment of Direct Air Capture as a Response to the Climate Crisis. *Nat. Commun.* **2021**, *12* (1), 1−13.
(26) Beuttler, C.; Charles, L.; Wurzbacher, J. The Role of Direct Air Capture in Mitigation of Anthropogenic Greenhouse Gas Emissions. *Frontiers in Climate* **2019**, *1*, 1−7.
(27) Sovacool, B. K.; Baum, C. M.; Low, S.; Roberts, C.; Steinhauser, J. Climate Policy for a Net-Zero Future: Ten Recommendations for Direct Air Capture. *Environmental Research Letters* **2022**, *17* (7), 074014.
(28) Nemet, G. F.; Callaghan, M. W.; Creutzig, F.; Fuss, S.; Hartmann, J.; Hilaire, J.; Lamb, W. F.; Minx, J. C.; Rogers, S.; Smith, P. Negative Emissions - Part 3: Innovation and Upscaling. *Environmental Research Letters* **2018**, *13* (6), 063003.
(29) Sanz-Pérez, E. S.; Murdock, C. R.; Didas, S. A.; Jones, C. W. Direct Capture of CO_2 from Ambient Air. *Chem. Rev.* **2016**, *116* (19), 11840−11876.
(30) Keith, D. W.; Holmes, G.; St. Angelo, D.; Heidel, K. A Process for Capturing CO_2 from the Atmosphere. *Joule* **2018**, *2* (8), 1573−1594.
(31) Welch, A. J.; Digdaya, I. A.; Kent, R.; Ghougassian, P.; Atwater, H. A.; Xiang, C. Comparative Technoeconomic Analysis of Renewable Generation of Methane Using Sunlight, Water, and Carbon Dioxide. *ACS Energy Letters* **2021**, 1540−1549.
(32) Jarimi, H.; Powell, R.; Riffat, S. Review of Sustainable Methods for Atmospheric Water Harvesting. *International Journal of Low-Carbon Technologies* **2020**, *15* (2), 253−276.
(33) Brambilla, A.; Gasparri, E.; Zolfaghari, L.; Keshavarzi, R.; Andaloro, A. On the Applicability of Atmospheric Water Harvesting Technologies on Building Facades: A Critical Review. *Journal of Cleaner Production* **2022**, *366* (June), 132809.
(34) Zhao, D.; Aili, A.; Zhai, Y.; Lu, J.; Kidd, D.; Tan, G.; Yin, X.; Yang, R. Subambient Cooling of Water: Toward Real-World Applications of Daytime Radiative Cooling. *Joule* **2019**, *3* (1), 111−123.
(35) Zhou, M.; Song, H.; Xu, X.; Shahsafi, A.; Xia, Z.; Ma, Z.; Kats, M. A.; Zhu, J.; Ooi, B. S.; Gan, Q.; Yu, Z. Accelerating Vapor Condensation with Daytime Radiative Cooling. *Proc. SPIE* **2019**, *1112107*, 6.
(36) European Commission. *A Hydrogen Strategy for a Climate Neutral Europe The Path towards a European Hydrogen Eco-System Step by Step* ; 2020, No. July.
(37) Brown, A.; Grünberg, N.*China's Nascent Green Hydrogen Sector: How Policy, Research and Business Are Forging a New Industry*; China Monitor, 2022.
(38) Kakoulaki, G.; Kougias, I.; Taylor, N.; Dolci, F.; Moya, J.; Jäger-Waldau, A. Green Hydrogen in Europe - A Regional Assessment: Substituting Existing Production with Electrolysis Powered by Renewables. *Energy Conversion and Management* **2021**, *228*, 113649.
(39) Lebrouhi, B. E.; Djoupo, J. J.; Lamrani, B.; Benabdelaziz, K.; Kousksou, T. Global Hydrogen Development - A Technological and Geopolitical Overview. *Int. J. Hydrogen Energy* **2022**, *47* (11), 7016−7048.
(40) García de Arquer, F. P.; Dinh, C. T.; Ozden, A.; Wicks, J.; McCallum, C.; Kirmani, A. R.; Nam, D. H.; Gabardo, C.; Seifitokaldani, A.; Wang, X.; Li, Y. C.; Li, F.; Edwards, J.; Richter, L. J.; Thorpe, S. J.; Sinton, D.; Sargent, E. H. CO_2 Electrolysis to Multicarbon Products at Activities Greater than 1 A Cm-2. *Science* **2020**, *367* (6478), 661−666.
(41) Xu, H.; Rebollar, D.; He, H.; Chong, L.; Liu, Y.; Liu, C.; Sun, C.-J.; Li, T.; Muntean, J. v; Winans, R. E.; Liu, D.-J.; Xu, T. Highly Selective Electrocatalytic CO_2 Reduction to Ethanol by Metallic Clusters Dynamically Formed from Atomically Dispersed Copper. *Nature Energy* **2020**, *5*, 623.
(42) Sullivan, I.; Goryachev, A.; Digdaya, I. A.; Li, X.; Atwater, H. A.; Vermaas, D. A.; Xiang, C. Coupling Electrochemical CO2 Conversion with CO_2 Capture. *Nature Catalysis* **2021**, *4* (11), 952−958.
(43) Dieterich, V.; Buttler, A.; Hanel, A.; Spliethoff, H.; Fendt, S. Power-to-Liquid via Synthesis of Methanol, DME or Fischer−Tropsch-Fuels: A Review. *Energy and Environmental Science. Royal Society of Chemistry* **2020**, *13*, 3207−3252.
(44) Vogt, C.; Monai, M.; Kramer, G. J.; Weckhuysen, B. M. The Renaissance of the Sabatier Reaction and Its Applications on Earth and in Space. *Nature Catalysis* **2019**, *2* (3), 188−197.
(45) Bailera, M.; Lisbona, P.; Romeo, L. M.; Espatolero, S.Power to Gas Projects Review: Lab, Pilot and Demo Plants for Storing Renewable Energy and CO_2. *Renewable and Sustainable Energy Reviews*; Elsevier Ltd, 2017; pp 292−312. DOI: 10.1016/j.rser.2016.11.130.
(46) Gido, B.; Friedler, E.; Broday, D. M. Liquid-Desiccant Vapor Separation Reduces the Energy Requirements of Atmospheric Moisture Harvesting. *Environ. Sci. Technol.* **2016**, *50* (15), 8362−8367.
(47) Smolinka, T.; Ojong, E. T.; Garche, J.Hydrogen Production from Renewable Energies-Electrolyzer Technologies. In *Electrochemical Energy Storage for Renewable Sources and Grid Balancing*; Elsevier Inc., 2015; pp 103−128. DOI: 10.1016/B978-0-444-62616-5.00008-5.
(48) Furler, P.Solar Thermochemical CO_2 and H_2O Splitting via Ceria Redox Reactions. *Doctoral Thesis*, Dep. Maschinenbau und Verfahrenstechnik, 2014, DOI: 10.3929/ethz-a-010207593.
(49) Lin, M.; Haussener, S. Solar Fuel Processing Efficiency for Ceria Redox Cycling Using Alternative Oxygen Partial Pressure Reduction Methods. *Energy* **2015**, *88*, 667−679.
(50) Marxer, D.; Furler, P.; Takacs, M.; Steinfeld, A. Solar Thermochemical Splitting of CO_2 into Separate Streams of CO and O2 with High Selectivity, Stability, Conversion, and Efficiency. *Energy Environ. Sci.* **2017**, *10* (5), 1142−1149.
(51) Zoller, S.; Koepf, E.; Nizamian, D.; Stephan, M.; Patané, A.; Haueter, P.; Romero, M.; González-Aguilar, J.; Lieftink, D.; de Wit, E.; Brendelberger, S.; Sizmann, A.; Steinfeld, A. A Solar Tower Fuel Plant for the Thermochemical Production of Kerosene from H_2O and CO2. *Joule* **2022**, *6* (7), 1606−1616.
(52) Pressure Swing Adsorption (PSA) Hydrogen Purification. https://www.airproducts.com/equipment/psa-hydrogen-purification#/ (accessed 2022-08-07).

(53) Hydrogen recovery and purification | Linde Engineering. https://www.linde-engineering.com/en/process-plants/adsorption-and-membrane-plants/hydrogen_recovery_and_purification/index.html (accessed 2022-08-07).
(54) Song, C.; Liu, Q.; Ji, N.; Deng, S.; Zhao, J.; Li, Y.; Song, Y.; Li, H. Alternative Pathways for Efficient CO2 Capture by Hybrid Processes—A Review. *Renewable and Sustainable Energy Reviews* **2018**, *82*, 215−231.
(55) Koytsoumpa, E. I.; Bergins, C.; Kakaras, E. The CO_2 Economy: Review of CO2 Capture and Reuse Technologies. *Journal of Supercritical Fluids* **2018**, *132*, 3−16.
(56) Dimitriou, I.; García-Gutiérrez, P.; Elder, R. H.; Cuéllar-Franca, R. M.; Azapagic, A.; Allen, R. W. K. Carbon Dioxide Utilisation for Production of Transport Fuels: Process and Economic Analysis. *Energy Environ. Sci.* **2015**, *8* (6), 1775−1789.
(57) Descoeudres, A.; Allebé, C.; Badel, N.; Barraud, L.; Champliaud, J.; Debrot, F.; Faes, A.; Lachowicz, A.; Levrat, J.; Nicolay, S.; Sansonnens, L.; Despeisse, M.; Ballif, C. Silicon Heterojunction Solar Cells: Towards Low-Cost High-Efficiency Industrial Devices and Application to Low-Concentration PV. *Energy Procedia* **2015**, *77*, 508−514.
(58) Lee, W. J.; Li, C.; Prajitno, H.; Yoo, J.; Patel, J.; Yang, Y.; Lim, S. Recent Trend in Thermal Catalytic Low Temperature CO_2 Methanation: A Critical Review. *Catal. Today* **2021**, *368*, 2−19.
(59) Yan, X.; Sun, W.; Fan, L.; Duchesne, P. N.; Wang, W.; Kübel, C.; Wang, D.; Kumar, S. G. H.; Li, Y. F.; Tavasoli, A.; Wood, T. E.; Hung, D. L. H.; Wan, L.; Wang, L.; Song, R.; Guo, J.; Gourevich, I.; Jelle, A. A.; Lu, J.; Li, R.; Hatton, B. D.; Ozin, G. A. Nickel@Siloxene Catalytic Nanosheets for High-Performance CO_2 Methanation. *Nat. Commun.* **2019**, *10* (1), na DOI: 10.1038/s41467-019-10464-x.
(60) Tountas, A. A.; Ozin, G. A.; Sain, M. M. Solar Methanol Energy Storage. *Nature Catalysis* **2021**, *4* (11), 934−942.
(61) Tackett, B. M.; Gomez, E.; Chen, J. G. Net Reduction of CO2 via Its Thermocatalytic and Electrocatalytic Transformation Reactions in Standard and Hybrid Processes. *Nature Catalysis* **2019**, *2* (5), 381−386.
(62) Luk, H. T.; Mondelli, C.; Ferré, D. C.; Stewart, J. A.; Pérez-Ramírez, J. Status and Prospects in Higher Alcohols Synthesis from Syngas. *Chemical Society Reviews* **2017**, *46*, 1358−1426.
(63) Cai, Y.; Fu, J.; Zhou, Y.; Chang, Y. C.; Min, Q.; Zhu, J. J.; Lin, Y.; Zhu, W. Insights on Forming N,O-Coordinated Cu Single-Atom Catalysts for Electrochemical Reduction CO2 to Methane. *Nat. Commun.* **2021**, *12*, 586.
(64) Wang, Z.; Yuan, Q.; Shan, J.; Jiang, Z.; Xu, P.; Hu, Y.; Zhou, J.; Wu, L.; Niu, Z.; Sun, J.; Cheng, T.; Goddard, W. A. Highly Selective Electrocatalytic Reduction of CO2into Methane on Cu-Bi Nano-alloys. *J. Phys. Chem. Lett.* **2020**, *11* (17), 7261−7266.
(65) Han, L.; Song, S.; Liu, M.; Yao, S.; Liang, Z.; Cheng, H.; Ren, Z.; Liu, W.; Lin, R.; Qi, G.; Liu, X.; Wu, Q.; Luo, J.; Xin, H. L. Stable and Efficient Single-Atom Zn Catalyst for CO_2 Reduction to CH_4. *J. Am. Chem. Soc.* **2020**, *142* (29), 12563−12567.
(66) Pan, H.; Barile, C. J. Electrochemical CO_2 Reduction to Methane with Remarkably High Faradaic Efficiency in the Presence of a Proton Permeable Membrane. *Energy Environ. Sci.* **2020**, *13* (10), 3567−3578.
(67) Zhang, Y.; Dong, L.-Z.; Li, S.; Huang, X.; Chang, J.-N.; Wang, J.-H.; Zhou, J.; Li, S.-L.; Lan, Y.-Q. Coordination Environment Dependent Selectivity of Single-Site-Cu Enriched Crystalline Porous Catalysts in CO_2 Reduction to CH_4. *Nat. Commun.* **2021**, *12*, 6390.
(68) Huang, J.; Hu, Q.; Guo, X.; Zeng, Q.; Wang, L. Rethinking $Co(CO_3)_{0.5}(OH)\cdot 0.11H_2O$: A New Property for Highly Selective Electrochemical Reduction of Carbon Dioxide to Methanol in Aqueous Solution. *Green Chem.* **2018**, *20* (13), 2967−2972.
(69) Yang, D.; Zhu, Q.; Chen, C.; Liu, H.; Liu, Z.; Zhao, Z.; Zhang, X.; Liu, S.; Han, B. Selective Electroreduction of Carbon Dioxide to Methanol on Copper Selenide Nanocatalysts. *Nat. Commun.* **2019**, *10*, 677.
(70) Mou, S.; Wu, T.; Xie, J.; Zhang, Y.; Ji, L.; Huang, H.; Wang, T.; Luo, Y.; Xiong, X.; Tang, B.; Sun, X. Boron Phosphide Nanoparticles: A Nonmetal Catalyst for High-Selectivity Electrochemical Reduction of CO 2 to CH 3 OH. *Adv. Mater.* **2019**, *31* (36), 1903499.
(71) Periasamy, A. P.; Ravindranath, R.; Senthil Kumar, S. M.; Wu, W. P.; Jian, T. R.; Chang, H. T. Facet- and Structure-Dependent Catalytic Activity of Cuprous Oxide/Polypyrrole Particles towards the Efficient Reduction of Carbon Dioxide to Methanol. *Nanoscale* **2018**, *10* (25), 11869−11880.
(72) Lu, L.; Sun, X.; Ma, J.; Yang, D.; Wu, H.; Zhang, B.; Zhang, J.; Han, B. Highly Efficient Electroreduction of CO_2 to Methanol on Palladium-Copper Bimetallic Aerogels. *Angew. Chem.* **2018**, *130* (43), 14345−14349.
(73) Geng, Z.; Kong, X.; Chen, W.; Su, H.; Liu, Y.; Cai, F.; Wang, G.; Zeng, J. Oxygen Vacancies in ZnO Nanosheets Enhance CO_2 Electrochemical Reduction to CO. *Angew. Chem.* **2018**, *130* (21), 6162−6167.
(74) Möller, T.; Ju, W.; Bagger, A.; Wang, X.; Luo, F.; Ngo Thanh, T.; Varela, A. S.; Rossmeisl, J.; Strasser, P. Efficient CO_2 to CO Electrolysis on Solid Ni-N-C Catalysts at Industrial Current Densities. *Energy Environ. Sci.* **2019**, *12* (2), 640−647.
(75) Jiao, J.; Lin, R.; Liu, S.; Cheong, W. C.; Zhang, C.; Chen, Z.; Pan, Y.; Tang, J.; Wu, K.; Hung, S. F.; Chen, H. M.; Zheng, L.; Lu, Q.; Yang, X.; Xu, B.; Xiao, H.; Li, J.; Wang, D.; Peng, Q.; Chen, C.; Li, Y. Copper Atom-Pair Catalyst Anchored on Alloy Nanowires for Selective and Efficient Electrochemical Reduction of CO_2. *Nat. Chem.* **2019**, *11* (3), 222−228.
(76) Zhang, H.; Li, J.; Xi, S.; Du, Y.; Hai, X.; Wang, J.; Xu, H.; Wu, G.; Zhang, J.; Lu, J.; Wang, J. A Graphene-Supported Single-Atom FeN 5 Catalytic Site for Efficient Electrochemical CO_2 Reduction. *Angew. Chem.* **2019**, *131* (42), 15013−15018.
(77) Nellaiappan, S.; Katiyar, N. K.; Kumar, R.; Parui, A.; Malviya, K. D.; Pradeep, K. G.; Singh, A. K.; Sharma, S.; Tiwary, C. S.; Biswas, K. High-Entropy Alloys as Catalysts for the CO_2 and CO Reduction Reactions: Experimental Realization. *ACS Catal.* **2020**, *10* (6), 3658−3663.
(78) Zhang, Y.; Li, K.; Chen, M.; Wang, J.; Liu, J.; Zhang, Y. Cu/Cu_2O Nanoparticles Supported on Vertically ZIF-L-Coated Nitrogen-Doped Graphene Nanosheets for Electroreduction of CO2 to Ethanol. *ACS Applied Nano Materials* **2020**, *3* (1), 257−263.
(79) Yuan, J.; Yang, M. P.; Zhi, W. Y.; Wang, H.; Wang, H.; Lu, J. X. Efficient Electrochemical Reduction of CO2 to Ethanol on Cu Nanoparticles Decorated on N-Doped Graphene Oxide Catalysts. *Journal of CO2 Utilization* **2019**, *33*, 452−460.
(80) Lv, K.; Fan, Y.; Zhu, Y.; Yuan, Y.; Wang, J.; Zhu, Y.; Zhang, Q. Elastic Ag-Anchored N-Doped Graphene/Carbon Foam for the Selective Electrochemical Reduction of Carbon Dioxide to Ethanol. *Journal of Materials Chemistry A* **2018**, *6* (12), 5025−5031.
(81) Wang, X.; Wang, Z.; García de Arquer, F. P.; Dinh, C. T.; Ozden, A.; Li, Y. C.; Nam, D. H.; Li, J.; Liu, Y. S.; Wicks, J.; Chen, Z.; Chi, M.; Chen, B.; Wang, Y.; Tam, J.; Howe, J. Y.; Proppe, A.; Todorović, P.; Li, F.; Zhuang, T. T.; Gabardo, C. M.; Kirmani, A. R.; McCallum, C.; Hung, S. F.; Lum, Y.; Luo, M.; Min, Y.; Xu, A.; O'Brien, C. P.; Stephen, B.; Sun, B.; Ip, A. H.; Richter, L. J.; Kelley, S. O.; Sinton, D.; Sargent, E. H. Efficient Electrically Powered CO_2-to-Ethanol via Suppression of Deoxygenation. *Nature Energy* **2020**, *5* (6), 478−486.
(82) Zhao, G.; Huang, X.; Wang, X.; Wang, X. Progress in Catalyst Exploration for Heterogeneous CO_2 Reduction and Utilization: A Critical Review. *Journal of Materials Chemistry A* **2017**, *5*, 21625−21649.
(83) Li, F.; MacFarlane, D. R.; Zhang, J. Recent Advances in the Nanoengineering of Electrocatalysts for CO_2 Reduction. *Nanoscale* **2018**, *10*, 6235−6260.
(84) Khan, K.; Tareen, A. K.; Aslam, M.; Zhang, Y.; Wang, R.; Ouyang, Z.; Gou, Z.; Zhang, H. Recent Advances in Two-Dimensional Materials and Their Nanocomposites in Sustainable Energy Conversion Applications. *Nanoscale* **2019**, *11* (45), 21622−21678.